Molecular Crystals and Liquid Crystals Science and Technology. Section A. Molecular Crystals and Liquid Crystals

Publication details, including instructions for authors and subscription information:
http://www.tandfonline.com/loi/gmcl19

Atomic Resolution Surface Imaging of Binary and Ternary Stage 1 Alkali Metal Graphite Intercalation Compounds by Scanning Tunneling Microscopy

H. P. Lang [a] , V. Thommen-geiser [a] & H.-J. Güntherodt [a]
[a] Univ. Basel, Condensed Matter Physics Dept., Basel, Switzerland

Version of record first published: 23 Oct 2006.

To cite this article: H. P. Lang , V. Thommen-geiser & H.-J. Güntherodt (1994): Atomic Resolution Surface Imaging of Binary and Ternary Stage 1 Alkali Metal Graphite Intercalation Compounds by Scanning Tunneling Microscopy, Molecular Crystals and Liquid Crystals Science and Technology. Section A. Molecular Crystals and Liquid Crystals, 244:1, 385-390

To link to this article: http://dx.doi.org/10.1080/10587259408050134

Mol. Cryst. Liq. Cryst. 1994, Vol. 244, pp. 385–390
Reprints available directly from the publisher
Photocopying permitted by license only

Printed in the United States of America

ATOMIC RESOLUTION SURFACE IMAGING OF BINARY AND TERNARY STAGE 1 ALKALI METAL GRAPHITE INTERCALATION COMPOUNDS BY SCANNING TUNNELING MICROSCOPY

H.P. LANG, V. THOMMEN-GEISER AND H.-J. GÜNTHERODT
Univ. Basel, Condensed Matter Physics Dept., Basel, Switzerland.

Abstract Li, K, Rb, Cs, KCs and RbCs graphite intercalation compounds of stage 1 are investigated by scanning tunneling microscopy in an inert-gas environment at 295 K. Various superlattice structures are identified such as 2×2, $\sqrt{3} \times \sqrt{3}$, $\sqrt{3} \times 3$, $\sqrt{3} \times 4$, $\sqrt{3} \times \sqrt{21}$, $\sqrt{3} \times \sqrt{27}$, $\sqrt{3} \times \sqrt{28}$ as well as incommensurate structures. Observed transformations between different superlattices are attributed to gradual loss of the intercalant.

INTRODUCTION

Graphite intercalation compounds (GIC's) represent model systems for layered conductors with electronic structures that can be widely altered by doping. Figure 1 schematically shows a GIC of stage 1 in side view (fig. 1a) and top view (fig. 1b). Several possible hexagonal superstructures in the graphene layers are indicated. Whereas the bulk structure of GIC's has already been extensively studied by X-ray diffraction, electron diffraction and transmission electron microscopy [1], a detailed study of the surface morphology of GIC's down to the atomic scale has been made possible only since the availability of high resolution local scanning probe methods such as scanning ion microscopy [2] and especially scanning tunneling microscopy (STM) [3–5]. In this paper, we concentrate on results obtained by STM on donor alkali metal GIC's in an inert-gas environment.

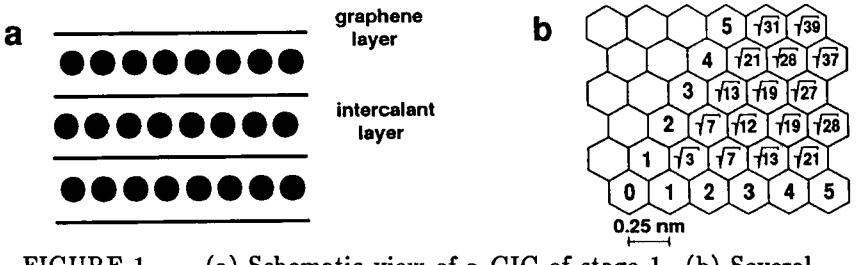

FIGURE 1. (a) Schematic view of a GIC of stage 1. (b) Several possible hexagonal superstructures on graphene layers.

EXPERIMENTAL

Li-, K-, and ternary KCs- and RbCs-GIC's of stage 1 are prepared by a liquid phase reaction of highly oriented pyrolitic graphite (HOPG) with the molten alkali metals in argon at 100-250 °C over 1-16 days. Rb- and Cs-GIC's of stage 1 are prepared by a two-zone gas phase reaction at 200-280 °C in 1-3 days. The stages of all samples is determined by X-ray diffraction.

STM is performed in a stainless-steel glove box filled with 1 bar of high-purity argon. A gas purification system lowers the O_2, N_2 and H_2O levels below our detection limit of 1 ppm. The GIC samples are sealed in glass tubes on a vacuum line following doping and introduced to the glove box through an evacuable air lock and therefore are never exposed to air. Prior to STM imaging, the samples are cleaved on the STM sample stage. We use mechanically prepared $Pt_{90}Ir_{10}$ tips, bias voltages between 10 and 300 mV, and tunneling currents between 0.5 and 10 nA [5]. The height information is encoded to a grey scale. The images represent raw data.

BINARY GRAPHITE INTERCALATION COMPOUNDS

The results obtained from binary GIC's of stage 1 are compiled in this section. By STM C_6Li exhibits flat terraces over a large scale and step heights of about 0.4 nm which correspond to the interlamellar distance of the graphene sheets ($I_c = 0.37$ nm). The ellipsoidally-shaped "darker" areas (apparent reduction of topographic height by 1-3 nm) in fig. 2a are possibly due to local deficiencies in lithium intercalant or are regions of increased local work function leading to an increased local tunneling barrier and therefore to an apparent decrease of the topographic height [5].

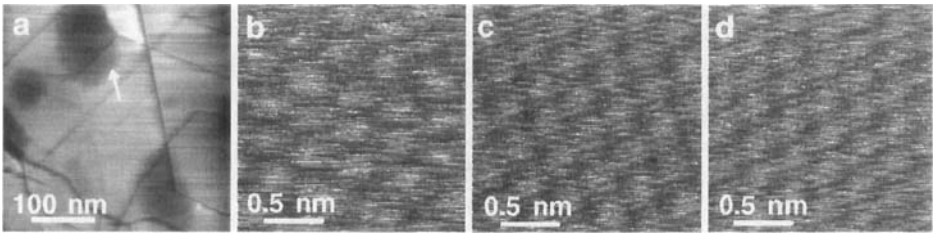

FIGURE 2. C_6Li: (a) Large scale STM image. The arrow marks an area of reduced topographic height. (b) Atomic resolution STM image showing a hexagonal 2 × 2 superlattice. (c) $\sqrt{3} \times \sqrt{3}$ superlattice. (d) incommensurate superlattice (lattice constant: 0.35 nm.)

Figures 2b-d show atomic resolution STM images of superstructures observed on C_6Li: a 2×2 (fig. 2b), a $\sqrt{3}\times\sqrt{3}$ (fig. 2c) and an incommensurate superstructure with a lattice constant of 0.35 $\pm$0.02 nm (fig. 2d). These results confirm the previous STM observations of three different hexagonal lattices on C_6Li [4-6].

C_8K exhibits by STM flat terraces (fig. 3a) with unit cell steps (0.6 nm in height, I_c = 0.54 nm). Again, line shaped regions of apparently increased topographic height (+0.2 nm) can be observed. They are possibly due to work function effects. Atomic resolution images show a 2×2 superstructure with the underlying graphite host lattice (fig. 3b), a $\sqrt{3} \times \sqrt{3}$ superlattice (fig. 3c) and a $\sqrt{3} \times \sqrt{27}$ modulation of the $\sqrt{3}\times\sqrt{3}$ superlattice (fig. 3d). During the course of STM imaging, a stepwise progression of first 2×2, $\sqrt{3} \times \sqrt{3}$, then $\sqrt{3} \times \sqrt{27}$ and finally graphite structures has been observed. This indicates a gradual depletion of the first gallery of C_8K during the measurement process within 20 min., likely due to a high surface reactivity and vapour pressure of K even in an inert-gas environment.

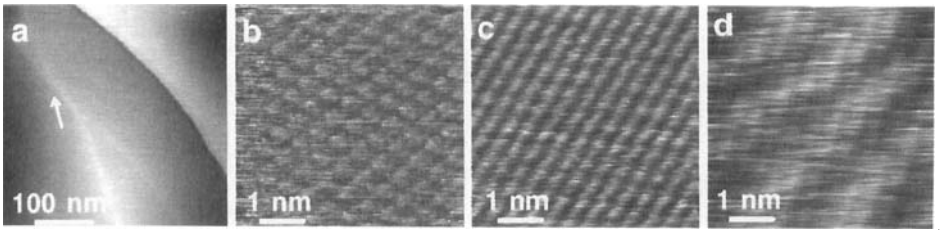

FIGURE 3. C_8K: (a) Large scale topography. The "bright" lines (arrow) are due to work function effects. (b) 2×2 superlattice with underlying graphite lattice. (c) $\sqrt{3} \times \sqrt{3}$. (d) $\sqrt{3} \times \sqrt{27}$ modulation.

C_8Rb and C_8Cs exhibit large terraces with 0.6 nm steps ($I_{c,Rb}$ = 0.56 nm, $I_{c,Cs}$ = 0.59 nm). Figure 4a shows a STM image of the surface of a C_8Cs sample. The "brighter" lines (arrow) are possibly boundaries between different intercalated domains. Figure 4b shows the C_8Cs 2×2 superlattice and fig. 4c displays the C_8Rb 2×2 superlattice. Note the vacancy and adatom defect (arrows) in fig. 4c. During the course of STM imaging, various one-dimensional superstructures have been observed. Two different spacings between linear structures can be observed in fig. 4d. The smaller spacing corresponds to a $\sqrt{3}\times3$ superlattice. The larger one is a $\sqrt{3}\times4$ structure. At even larger depletion of the first gallery of C_8Cs, linear $\sqrt{3}\times\sqrt{21}$ (fig. 4e) or linear superstructures with two different spacings ($\sqrt{3}\times\sqrt{21}/\sqrt{3}\times\sqrt{28}$) (fig. 4f) are observed simultaneously with the graphite host lattice.

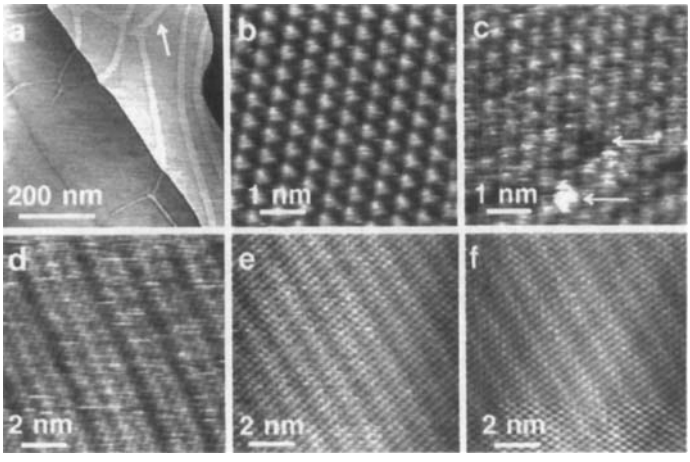

FIGURE 4. (a) Large scale STM image of a C_8Cs surface. Note the "brighter" lines (arrow) which are possibly boundaries between different intercalated domains. (b) C_8Cs 2×2. (c) C_8Rb 2×2. (d) Cs-GIC: linear superstructures $\sqrt{3} \times 3$, $\sqrt{3} \times 4$. (e) $\sqrt{3} \times \sqrt{21}$. (f) $\sqrt{3} \times \sqrt{21}$, $\sqrt{3} \times \sqrt{28}$.

TERNARY GRAPHITE INTERCALATION COMPOUNDS

KCs- and RbCs-GIC's have been studied as an extension of the work on binary alkali metal GIC's. Similar superlattices as in binary GIC's are expected.

KCs-GIC's (stage 1) exhibit on a larger scale similar structures as K- and Cs-GIC's of stage 1. The STM image in fig. 5a shows, in addition to step structures, ellipsoidally-shaped islands (arrow) of greater height (even across steps). We attribute these islands to an inhomogeneous distribution of the intercalant that

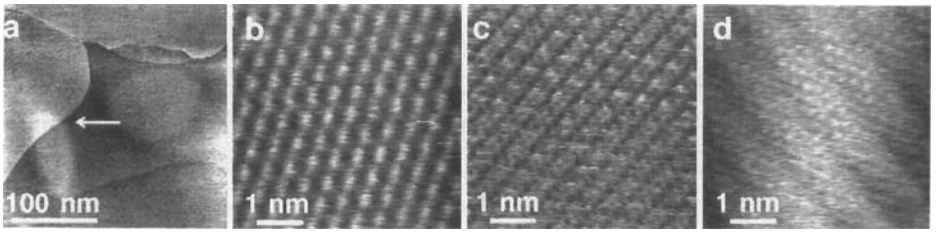

FIGURE 5. (a) KCs-GIC: large scale STM image. Note the ellipoidally-shaped islands of increased topographic height (0.5 nm, see arrow) that are attributed to a inhomogeneous distribution of the intercalant. (b) 2×2. (c) 2×2 and graphite lattice. (d) $\sqrt{3} \times 4$.

would result in the observed electronic effect. Figures 5b and 5c show two different types of 2×2 superlattices. In fig. 5c the graphite host lattice can be observed while in fig. 5b only the intercalant is imaged. No distinction between the different alkali metals is possible. Figure 5d shows a one-dimensional linear $\sqrt{3} \times 4$ structure and the graphite host lattice.

RbCs-GIC's show analogous structures to those observed in KCs-GIC's. A grain boundary is marked by an arrow in the large scale image of a RbCs-GIC. The topographic height difference between the two grains is 0.55 nm (slightly smaller than the interlamellar spacing). Figure 6b displays a 2×2 superlattice. Fig. 6c additionally shows the underlying graphite host lattice. Figure 6d shows the linear $\sqrt{3} \times 4$ superlattice which is only found at a later stage of the STM experiment (similar to K-, Cs-, Rb- and KCs-GIC's).

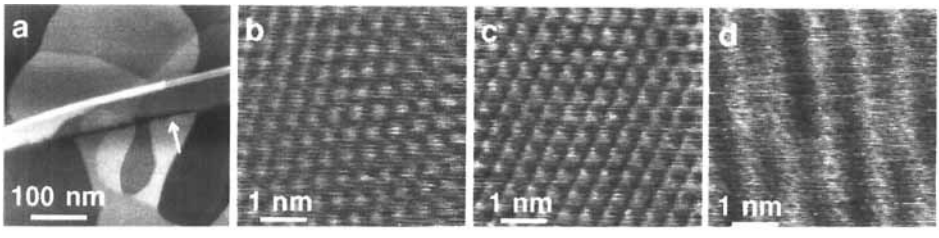

FIGURE 6. RbCs-GIC: (a) large scale STM image (step heights: 0.6 and 1.1 nm). A grain boundary is marked by an arrow. (b) 2×2 superlattice. (c) 2×2 and graphite lattice. (d) $\sqrt{3} \times 4$ superlattice that evolved with time.

DISCUSSION AND SUMMARY

The various superlattice structures observed in binary and ternary alkali-metal GIC's of stage 1 and the steady evolution with time from denser $\sqrt{3} \times \sqrt{3}$ and 2×2 packing, over more dilute one-dimensional linear structures such as $\sqrt{3} \times 3$ to no superstructures at all are strong indications of the intercalant depletion in the first gallery of the GIC's. Although the STM experiments are performed in an argon-filled glove box with very low impurity levels (see experimental section), some intercalant may evaporate from the GIC sample. This continuous emptying of the first gallery causes the observed structural transformations with time. The high vapour pressures of the alkali metals renders impossible the investigation of these GIC's in ultrahigh vacuum.

Li-GIC's of stage 1, however, are believed to exhibit a Li metal top surface layer [4,5] for the following reasons: first, the graphite host lattice could never be simultaneously imaged with the superlattice; and second, the measured corrugation amplitudes are much smaller than those of other alkali-metal GIC's and compare better to those of a metal.

The heavier alkali-metal GIC's most likely have a graphitic top surface layer since cleavage of these compounds leaves surfaces only partially covered by alkali-metal which is likely to evaporate off in the inert gas environment. Two processes could be responsible for the image contrast in the STM images. First, the intercalant layers directly influence the electronic density of states near the Fermi level and the electronic structure of the GIC's is imaged by STM; or second, the underlying intercalant layer causes a buckling of the top graphite layer and the topographic structure is imaged. Both effects may contribute to the actual STM image, but at present, they cannot be easily separated.

In conclusion, STM has proven to be a valuable tool for the study of the surface of alkali-metal GIC's with atomic resolution.

Acknowledgements. We would like to thank R. Wiesendanger, J. Frommer, D. Anselmetti and G. Overney for helpful discussions. We are grateful to A.W. Moore (Union Carbide) for generously providing HOPG samples. The Swiss National Science Foundation is acknowledged for financial support.

REFERENCES

1. H. Zabel and S.A. Solin, Graphite Intercalation Compounds I (Springer-Verlag, New York, 1990), Springer Series in Materials Science Vol. 14.
2. R. Levi-Setti, G. Crow, Y.L. Wang, N.W. Parker, R. Mittleman and D.M. Hwang, Phys. Rev. Lett., 54, 2615 (1985).
3. S. Gauthier, S. Rousset, J. Klein, W. Sacks and M. Belin, J. Vac. Sci. Technol., A 6, 360 (1988).
4. D. Anselmetti, R. Wiesendanger and H.-J Güntherodt, Phys. Rev. B, 39, 11135 (1989).
5. H.P. Lang, R. Wiesendanger, V. Thommen-Geiser and H.-J Güntherodt, Phys. Rev. B, 45, 1829 (1992).
6. D. Anselmetti, V. Geiser, G. Overney, R. Wiesendanger and H.-J Güntherodt, Phys. Rev. B, 42, 1848 (1990).